MULTILEVEL MODEL ORDER REDUCTION WITH GENERALIZED COMPRESSION OF BOUNDARIES FOR 3-D FEM ELECTROMAGNETIC ANALYSIS

Grzegorz Fotyga, Krzysztof Nyka*, and Michal Mrozowski

Faculty of Electronics, Telecommunications and Informatics (ETI), Gdansk University of Technology, Gdansk 80-233, Poland

Abstract—This paper presents a multilevel Model Order Reduction technique for a 3-D electromagnetic Finite Element Method analysis. The reduction process is carried out in a hierarchical way and involves several steps which are repeated at each level. This approach brings about versatility and allows one to efficiently analyze complex electromagnetic structures. In the proposed multilevel reduction the entire computational domain is covered with macro-elements which are subsequently nested, in such a way that size of the problem which has to be reduced at each level is relatively small. In order to increase the speed of the reduction at each level, the electric field at the macro-elements' boundaries is projected onto the subspace spanned by Legendre polynomials and trigonometric functions. The results of the numerical experiments confirm the validity and efficiency of the presented approach.

1. INTRODUCTION

The finite element method (FEM) is one of the most versatile mesh-based numerical techniques used nowadays to solve electromagnetic problems in geometrically complex structures. However, it becomes rather time and memory consuming when analyzing multiscale problems which require strong local mesh refinements. One emerging trend to reduce the simulation time is to use Graphics Processing Units combined with matrix solvers [1, 2]. Another way to improve the efficiency of FEM in such cases is to apply model order reduction (MOR) techniques which since the end of the last century have been

gaining popularity in the area of computational electromagnetics. In particular, MOR has been successfully adopted in mesh based methods such as the FEM [3–8] and the finite difference methods, both in time (FDTD) and frequency (FDFD) domain [9–12]. The main idea of MOR is to find a low-dimensional approximation (subspace) of the original large set of state-space equations which provides satisfactory accuracy of the computations as far as the input-output behavior of the circuit is concerned [13]. In other words, huge sparse FEM matrices are replaced with small but dense ones. Since the original number of variables of the problem is reduced significantly, there are two main benefits of this operation: a considerable acceleration of computations and decrease in memory requirements. The reduction process involves repetitive solution of a system of original equations at a single (or few) frequency point, which can be done with a single LU decomposition, and pays off when wideband calculations are needed. However, since the original system has to be solved in order to find the projection basis, the size of the matrix limits the applicability of the technique. One area in which the MOR technique is particularly useful and its benefits are not offset by the matrix size, is when it is applied locally to subregions which require strong mesh refinements, due to a complex electromagnetic field distribution. The small and dense matrix blocks corresponding to these subregions are called either macromodels or macro-elements [3, 9].

Even though the matrices processed for finding the projection basis are much smaller than the matrix for the entire domain, creating macro-elements usually becomes a decisive numerical load, which increases with the volume of the subregions subject to MOR and the number of the unknowns at their boundaries. This is particularly relevant in 3-D problems and may affect the overall computational efficiency. To remedy this, the projection of the field at the boundaries onto orthogonal functions prior to reduction was proposed in [5, 10]. In our recent paper [3] we have developed a formulation of the approach introduced in [4] adapted for a 3-D FEM and demonstrated the benefits of using this approach for the cascaded waveguide structures. The approach described therein combines the efficient model order reduction (ENOR) algorithm [14] with modal expansion at the interfaces between the subdomains [9]. Since used to connect macro-elements to an adjacent mesh or another macro-element these interfaces are also called macro-element ports. The creation of the macro-elements is preceded by projecting the field at their ports onto a subspace spanned by a few waveguide modes. The number of modes which have to be taken into account is small, as higher order modes excited at a waveguide discontinuity decay quickly and can be

neglected. This step results in much lower number of the degrees of freedom at macro-elements' ports, therefore can be referred to as port compression.

Although the method proposed in [3] improves the speed of the analysis, it still has some limitations which will be addressed in this paper. Since only waveguide modes are used for the expansion of the tangential fields of the macro-elements' ports they have to be located at the cross-section of a waveguide and constrained by metallic walls (PEC). Another limitation becomes apparent if one considers many macro-elements. If there are many macro-elements and/or their dense matrices are not sufficiently small, the resulting system may remain large enough to make its solution a considerable component of the overall computational load.

In this paper we propose two enhancements to the MOR technique in the 3-D FEM analysis which overcome the above mentioned limitations. To improve the efficiency of solving the reduced system we use the multilevel model order reduction which extends the standard single-level MOR by introducing a hierarchical grouping of subregions subject to subsequent multiple order reductions. A similar approach was proposed for the 2-D FD formulations in [12]. The macro-elements created at lower levels are repeatedly embedded in upper-level macro-elements. At the top level only one macro-element remains which corresponds to the whole domain. In order to relax the restrictions regarding the division of the analyzed problem into subdomains, which are imposed by the need of modal expansion of the fields at their interfaces, we propose a more general formulation of the compression of macro-elements' ports. Instead of waveguide modes we use series of orthogonal functions which allows for separation of macro-elements from the physical boundaries of an analyzed structure. The same idea has been used in the FDFD method [9], however only for 2-D problems. In this paper Legendre polynomials and trigonometric functions are applied to a full 3-D vectorial FEM approximation.

2. FORMULATION

2.1. Finite Element Method

Let us consider a source-free bounded 3-D region Ω. A part of the region's boundary is a perfect electric conductor, while the remaining parts form input or output ports where excitation is applied. The electric field $\vec{E}$ obeys the vector wave equation [3, 15]:

$$\nabla \times \frac{1}{\mu_r} \nabla \times \vec{E} - k_0^2 \epsilon_r \vec{E} = 0 \tag{1}$$

where $\vec{E}$ is the vector of the electric field, k_0 the wavenumber, and μ_r, ϵ_r are the relative permittivity and permeability of the medium, respectively. Due to the FEM approximation of (1) using curvilinear tetrahedral elements and the third order vector basis functions [16] and applying perfect electric conductor surface (PEC) on all physical walls, the following matrix equation is obtained [17]:

$$\left(\mathbf{K} - k_0^2 \mathbf{M}\right)\mathbf{e} = \mathbf{b}, \qquad (2)$$

where $\mathbf{K}$ and $\mathbf{M}$ are $N_0 \times N_0$ sparse symmetric stiffness and mass matrices, respectively. $\mathbf{e}$ is the vector of unknown coefficients of the basis functions associated with mesh edges, faces and elements, $\mathbf{b}$ the excitation vector, and N_0 the total number of degrees of freedom. Since there are N_0 degrees of freedom and the problem is assumed to lossless, the solution of Equation (2) is sought in a R^{N_0} space. To indicate that the solution is related to the region Ω, we shall denote $\underline{\Omega}$ the linear subspace related to the degrees of freedom associated with this region. The same notation will be used regarding all subregions and their corresponding solution subspaces.

2.2. Model Order Reduction Algorithm

For the sake of simplicity we will introduce the model-order reduction algorithm for a generic problem with a source-free 3-D region $\widehat{\Omega}$ (Figure 1) with $\widehat{N}$ variables, which will be subject to the reduction scheme. It is bounded by metallic walls and input-output ports $P_1 \ldots P_N$. Such a model problem may also represent a situation where $\widehat{\Omega}$ is a subregion of a larger region Ω, and consequently $\widehat{N} \leq N_0$. In this case physical metallic boundaries may not exist, and the boundary is composed of fictitious interfaces between subregions. Our MOR approach, whose details were presented in [3, 8], begins with a consistent numbering of the global variables in order to split the
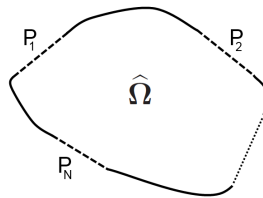

Figure 1. A source-free domain $\widehat{\Omega}$, bounded by the metallic walls and input-output ports $P_1 \ldots P_N$.

matrices and vectors from (2) into the following blocks:

$$\left(\begin{bmatrix} \mathbf{K}_P & \widehat{\mathbf{S}}_K^T \\ \widehat{\mathbf{S}}_K & \widehat{\mathbf{K}} \end{bmatrix} + k_0^2 \begin{bmatrix} \mathbf{M}_P & \widehat{\mathbf{S}}_M^T \\ \widehat{\mathbf{S}}_M & \widehat{\mathbf{M}} \end{bmatrix}\right) \begin{bmatrix} \mathbf{e}_P \\ \widehat{\mathbf{e}} \end{bmatrix} = \begin{bmatrix} \mathbf{b}_P \\ 0 \end{bmatrix}, \quad (3)$$

where index P and a hat denote the blocks which correspond to the ports and to the $\widehat{\Omega}$ region, respectively. Submatrices $\widehat{\mathbf{S}}_K$ and $\widehat{\mathbf{S}}_M$ correspond to the elements which couple region $\widehat{\Omega}$ to the rest of the computational domain. Equation (3) can be split into two matrix equations, one of which has the form:

$$\left(\widehat{\mathbf{K}} + k_0^2 \widehat{\mathbf{M}}\right)\widehat{\mathbf{e}} = -\left(\widehat{\mathbf{S}}_K + k_0^2 \widehat{\mathbf{S}}_M\right)\mathbf{e}_P. \quad (4)$$

Note that the above equation involves the degrees of freedom corresponding to region $\widehat{\Omega}(\widehat{\mathbf{e}})$ or to ports ($\mathbf{e}_P$). Vector $\mathbf{b}_P$ serves as the excitation. The equation has the form which is suitable for application of the ENOR [14] algorithm which can be applied in order to reduce the number of variables in region $\widehat{\Omega}$:

$$\left(s_0 \mathbf{C} + \frac{1}{s_0}\Gamma\right)\widehat{\mathbf{e}} = \mathbf{B}_e \mathbf{e}_P, \quad (5)$$

where $\mathbf{C} = \widehat{\mathbf{M}}$, $\Gamma = \widehat{\mathbf{K}}$, $\mathbf{B}_e = -(s_0^{-1}\widehat{\mathbf{S}}_K + s_0\widehat{\mathbf{S}}_M)$ and $s_0 = k_0$. The ENOR algorithm generates a frequency-independent set of orthonormal vectors, called basis $\mathbf{V}$, which spans the solution space which is sufficient to faithfully reflect the interaction between fields at ports in limited frequency range. The number of columns in $\mathbf{V}$ depends on q — the reduction order and N_P — the number of variables at the macro-element interface, and it is equal to:

$$\widetilde{N} = q N_P. \quad (6)$$

Note that $\widetilde{N} \ll \widehat{N}$. The value of q and N_P has a strong impact on the efficiency of the reduction algorithm [3]. The choice of an expansion frequency s_0 [14] depends on the bandwidth of the analyzed structure and in our case it is set to $2\pi f_0$, where f_0 is the center frequency. The last step of the MOR algorithm is the projection of the second equation in (3) using $\mathbf{V}$, which results in a significant reduction of the number of variables:

$$\left(\begin{bmatrix} \mathbf{K}_P & \widehat{\mathbf{S}}_K^T \mathbf{V} \\ \mathbf{V}^T \widehat{\mathbf{S}}_K & \mathbf{V}^T \widehat{\mathbf{K}} \mathbf{V} \end{bmatrix} + k_0^2 \begin{bmatrix} \mathbf{M}_P & \widehat{\mathbf{S}}_M^T \mathbf{V} \\ \mathbf{V}^T \widehat{\mathbf{S}}_M & \mathbf{V}^T \widehat{\mathbf{M}} \mathbf{V} \end{bmatrix}\right) \begin{bmatrix} \mathbf{e}_P \\ \mathbf{V}^T \widehat{\mathbf{e}} \end{bmatrix} = \begin{bmatrix} \mathbf{b}_P \\ \mathbf{0} \end{bmatrix}. \quad (7)$$

After substituting:

$$\widetilde{\mathbf{K}} = \mathbf{V}^T \widehat{\mathbf{K}} \mathbf{V}, \ \widetilde{\mathbf{M}} = \mathbf{V}^T \widehat{\mathbf{M}} \mathbf{V}, \ \widetilde{\mathbf{S}}_K = \mathbf{V}^T \widehat{\mathbf{S}}_K, \ \widetilde{\mathbf{S}}_M = \mathbf{V}^T \widehat{\mathbf{S}}_M, \ \widetilde{\mathbf{e}} = \mathbf{V}^T \widehat{\mathbf{e}} \quad (8)$$

one obtains:

$$\left(\left[\begin{array}{cc} \mathbf{K}_P & \widetilde{\mathbf{S}}_K^T \\ \widetilde{\mathbf{S}}_K & \widetilde{\mathbf{K}} \end{array}\right] + k_0^2 \left[\begin{array}{cc} \mathbf{M}_P & \widetilde{\mathbf{S}}_M^T \\ \widetilde{\mathbf{S}}_M & \widetilde{\mathbf{M}} \end{array}\right]\right)\left[\begin{array}{c} \mathbf{e}_P \\ \widetilde{\mathbf{e}} \end{array}\right] = \left[\begin{array}{c} \mathbf{b}_P \\ 0 \end{array}\right], \qquad (9)$$

where the tilde represents the reduction of the matrix operators $\widehat{\mathbf{M}}$, $\widehat{\mathbf{K}}$, $\widehat{\mathbf{S}}_K$, $\widehat{\mathbf{S}}_M$ and the vector of unknowns $\widehat{\mathbf{e}}$ by the projection vectors $\mathbf{V}$. As the effect of the projection, the number of elements in $\widetilde{\mathbf{e}}$ is equal to $\widetilde{N}$, which is much smaller than $\widehat{N}$. The reduction process associated with region $\widehat{\Omega}$, described above can be represented as follows:

$$\left(\underline{\widehat{\Omega}}, \underline{P}\right) \xrightarrow{\text{projection } \mathbf{V}} \left(\underline{\widetilde{\Omega}}, \underline{P}\right), \qquad (10)$$

where the solution subspace $\underline{\widehat{\Omega}}$, with $\widehat{N}$ degrees of freedom, is projected onto $\underline{\widetilde{\Omega}}$ of size $\widetilde{N}$, using the orthogonal basis $\mathbf{V}$, whereas the electric fields at the ports $\underline{P}$ remain unchanged (note, that $\underline{\widehat{\Omega}}$ and $\underline{P}$ denotes the solution subspaces of subregions $\widehat{\Omega}$ and P, respectively). Although the presented MOR procedure was performed for the whole domain, it can be applied separately to many subdomains of more complex problems. For such realistic situations a multilevel reduction is proposed with the aim of further improving the efficiency of model-order reduction.

2.3. Multilevel Model Order Reduction

Let us consider a structure (Figure 2(a)) composed of the two cavities Ω_1 and Ω_2, separated by the internal port P_8, with four input-output ports $P_1 \ldots P_4$. Each of the cavities contains small geometrical features, which cause complex field behavior in their surroundings. Such structure can be analyzed by means of the approach presented in [3], using the modal projection in ports $\underline{P_1} \ldots \underline{P_4}$ and $\underline{P_8}$ and creating two macro-elements, which cover the whole computational domain. However, such an analysis might be inefficient, since the number of variables in each of the cavities can be too large, affecting the reduction time. In order to alleviate this effect we propose to apply reduction in a hierarchical way, starting from relatively small regions (possibly not connected) and then gradually extending the scope of the region which is to be subject to reduction up to the point where the entire structure is converted into a single macro-element. In other words, the reduction process is divided into steps forming a procedure which is illustrated in (Figure 2). After [12] we call it a multilevel reduction.

These steps of the reduction form a multilevel hierarchy, where macro-elements created at lower levels are repeatedly embedded in upper-level macro-elements. In the first step, corresponding to the
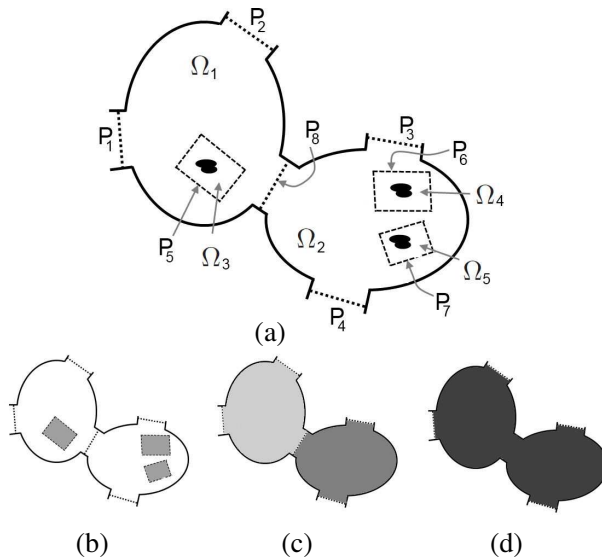
Figure 2. The structure subject to (a) the multilevel reduction approach and (b)–(d) three stages of subsequent levels of the reductions. The shades of grey indicate the subregions covered by macro-elements created at different levels.

lowest level (Figure 2(b)) regions with the finest mesh ($\Omega_3 \ldots \Omega_5$) should be separated from the computational domain using artificial interfaces $P_5 \ldots P_7$. They are then subject to the MOR procedure carried out in the manner presented in Section 2.2. It should be noted that the procedure based on modal expansion, which was presented in [3], cannot be used to accelerate the reduction process. This is because the fictitious interfaces are not connected to a physical boundary of the structure so the modes can not be defined. For such cases a more general approach was developed, which is presented in the subsequent sections of this paper. In the second step (Figure 2(c)) the FEM equations for each of the cavities are reduced, creating two macro-elements, however each of them is composed of the parts reduced in the first step and the parts which have not been reduced yet ($\underline{\Omega_1}$, $\underline{\Omega_2}$). In the last step all macro-elements which were created previously are gathered together creating a single macro-element for the whole structure (Figure 2(d)).

Each of the multilevel reduction stages can be described using the

following transformation, according to (10):

$$\left(\widehat{\underline{\Omega}}^{(l)}, \underline{P}^{(l)}\right) \xrightarrow{\text{projection } \mathbf{V}} \left(\widetilde{\underline{\Omega}}^{(l)}, \underline{P}^{(l)}\right), \tag{11}$$

where the uppercase index l denotes the reduction level. Using this notation different multilevel schemes may be expressed in a very compact form which, for the problem illustrated in Figure 2, is as following:

- $l = I$ — three macro-elements:

$$\begin{aligned}
\widehat{\underline{\Omega}}^{(Ia)} &= \underline{\Omega}_3, & \underline{P}^{(Ia)} &= \underline{P}_5, \\
\widehat{\underline{\Omega}}^{(Ib)} &= \underline{\Omega}_4, & \underline{P}^{(Ib)} &= \underline{P}_6, \\
\widehat{\underline{\Omega}}^{(Ic)} &= \underline{\Omega}_5, & \underline{P}^{(Ic)} &= \underline{P}_7.
\end{aligned} \tag{12}$$

- $l = II$ — two macro-elements:

$$\begin{aligned}
\widehat{\underline{\Omega}}^{(IIa)} &= (\underline{\Omega}_1 \cup \underline{P}_5) \cup \widetilde{\underline{\Omega}}^{(Ia)}, & \underline{P}^{(IIa)} &= \underline{P}_1 \cup \underline{P}_2 \cup \underline{P}_8, \\
\widehat{\underline{\Omega}}^{(IIb)} &= (\underline{\Omega}_2 \cup \underline{P}_6 \cup \underline{P}_7) \cup \widetilde{\underline{\Omega}}^{(Ib)} \cup \widetilde{\underline{\Omega}}^{(Ic)}, & \underline{P}^{(IIb)} &= \underline{P}_3 \cup \underline{P}_4 \cup \underline{P}_8.
\end{aligned} \tag{13}$$

- $l = III$ — one macro-element:

$$\underline{\Omega}^{(III)} = \widetilde{\underline{\Omega}}^{(IIa)} \cup \widetilde{\underline{\Omega}}^{(IIb)} \cup \underline{P}_8, \ \underline{P}^{(III)} = \underline{P}_1 \cup \underline{P}_2 \cup \underline{P}_3 \cup \underline{P}_4. \tag{14}$$

2.4. Orthogonal Projection at Macro-element Interfaces

As stated in Subsection 2.2, the size of a macro-element $\widetilde{N} \times \widetilde{N}$, as well as the efficiency of the reduction process depends on q and N_P — the number of FEM variables at the interface that couple the macro-element to its surroundings. The value of N_P can be decreased by means of the operation called the orthogonal projection [3, 9, 10], which is applied prior to the MOR procedure. In order to proceed with the description of orthogonal projection the tangential electric field $\vec{E}_t^{(k)}$ at the port P_k in the local coordinates (q_1, q_2) and corresponding unit vectors $(\vec{i_1}, \vec{i_2})$ is expanded into a series of orthogonal functions:

$$\vec{E}_t^{(k)}(q_1, q_2) = \sum_{i=0}^{N_{1i}^{(k)}} \vec{i_1} a_{1i}^{(k)} e_{1i}(q_1, q_2) + \sum_{j=0}^{N_{2j}^{(k)}} \vec{i_2} a_{2j}^{(k)} e_{2j}(q_1, q_2). \tag{15}$$

In terms of 2-D FEM edge basis functions at the port P_k it can be expressed in the the following vectorial form:

$$\mathbf{E}_t^{(k)} = \sum_{i=1}^{N'_{Pk}} a_i^{(k)} \mathbf{e}_{t,i}^{(k)} \tag{16}$$

where k and i denote port and mode indices, respectively, $a_i^{(k)}$ is the amplitude of the i-th orthogonal basis vector $\mathbf{e}_{t,i}^{(k)}$ discretized on a 2-D FEM mesh. The expansion (16) is truncated to only a few low-order terms that have the strongest impact on the solution accuracy, therefore $N'_{Pk} \ll N_{Pk}$, where N_{Pk} is the number of unknown FEM coefficients at the port P_k.

The orthogonal projection of the tangential electric fields at each port P_k is performed by means of the projection basis $\mathbf{E}_{Pk}$ comprising N'_{Pk} rows of orthogonal vectors $\mathbf{e}_{t,i}^{(k)}$ of the lengths N_{Pk}. As a result, N_{Pk} unknown coefficients of the FEM basis functions in vectors $\mathbf{e}_{Pk}$ are replaced with vectors $\mathbf{e}'_{Pk} = \mathbf{E}_{Pk}^T \mathbf{e}_{Pk}$, each of them comprising N'_{Pk} unknown amplitudes $a_i^{(k)}$ of the orthogonal basis $\mathbf{e}_{t,i}^{(k)}$. These vectors can be combined together for all ports $P_1, \ldots, P_N$ and written in a compact form as:

$$\mathbf{e}_P = [\mathbf{e}_{P1} \ldots \mathbf{e}_{Pk} \ldots \mathbf{e}_{P_N}]^T \longrightarrow \mathbf{e}'_P = [\mathbf{e}'_{P1} \ldots \mathbf{e}'_{Pk} \ldots \mathbf{e}'_{P_N}]^T . \quad (17)$$

The lengths of the above vectors are:

$$N_P = \sum_{k=1}^{N} N_{Pk} \longrightarrow N'_P = \sum_{k=1}^{N} N'_{Pk} \quad (18)$$

The system resulting from the orthogonal projection for combined unknowns (17) is derived from the initial FEM system (3):

$$\left(\begin{bmatrix} \mathbf{K}'_P & \widehat{\mathbf{S}}'^T_K \\ \widehat{\mathbf{S}}'_K & \widehat{\mathbf{K}} \end{bmatrix} + k_0^2 \begin{bmatrix} \mathbf{M}'_P & \widehat{\mathbf{S}}'^T_M \\ \widehat{\mathbf{S}}'_M & \widehat{\mathbf{M}} \end{bmatrix} \right) \begin{bmatrix} \mathbf{e}'_P \\ \widehat{\mathbf{e}} \end{bmatrix} = \begin{bmatrix} \mathbf{b}'_P \\ 0 \end{bmatrix} , \quad (19)$$

where

$$\mathbf{K}'_P = \mathbf{E}_P^T \mathbf{K}_P \mathbf{E}_P, \ \mathbf{M}'_P = \mathbf{E}_P^T \mathbf{M}_P \mathbf{E}_P, \ \widehat{\mathbf{S}}'_K = \mathbf{E}_P^T \widehat{\mathbf{S}}_K, \ \widehat{\mathbf{S}}'_M = \mathbf{E}_P^T \widehat{\mathbf{S}}_M \quad (20)$$

The subsequent model-order reduction is performed according to the same procedure as the one presented in Equations (3)–(9) after introducing the primed elements derived above. Since $N'_{Pk} \ll N_{Pk}$ and consequently $N'_P \ll N_P$ the projection significantly reduces the number of unknowns at the ports of a macro-element, the column rank of orthonormal basis $\mathbf{V}$ as well as the resulting size of a macro-element:

$$\widetilde{N}' = q N'_P \ll \widetilde{N}, \quad \text{where} \quad \widetilde{N} = q N_P. \quad (21)$$

2.4.1. Modal Expansion

The ports bounded by physical boundaries may be considered as cross-sections of short waveguides. Referring to Figure 2 this takes place for

ports $P_1 \ldots P_4$ and P_8. In such cases the distribution of the tangential electric field at the ports can be expressed as a modal expansion based on orthogonal waveguide TE and TM modes. This case was considered in [3]. The modal basis is computed at each port separately, either analytically, or numerically as a solution of a 2-D vector FEM eigenvalue problem. In the current paper the modal basis is derived analytically. Once the model basis has been determined, the next step is the projection onto the 2-D FEM basis. This is done using a general framework outlined in the next section.

2.4.2. Functional Expansion

As noted in the introduction, the modal expansion restricts the applicability of compression of macro-element boundaries to the situation where the port is a cross-section of a waveguide. Greater flexibility can be achieved if we admit that the port is not associated with a waveguide, but it is just a fictitious interface introduced inside the computational domain. Examples of such generalized ports are contours P_5, P_6 and P_7 given in Figure 2. To explain the port compression procedure for such cases we shall use an example. Figure 3 shows a discontinuity sandwiched between two PEC planes. The discontinuity causes complex field distribution in its surroundings. In order to perform MOR locally in the vicinity of this discontinuity we separate it from the rest of the computational domain using four fictitious interfaces $P_1 \ldots P_4$ serving as the macro-element ports. Since these ports do not extend to the physical boundaries of the domain, a modal expansion can not be applied. However, if the interfaces are chosen in such a way that they conform to the constant-value planes of a local rectangular (or any other separable) coordinate system, the expansion in each dimension can be performed independently using
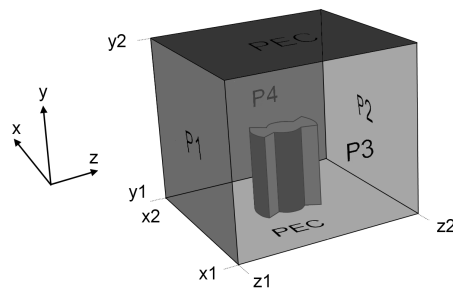

Figure 3. The discontinuity bounded by four fictitious interfaces $P_1 \ldots P_4$ and two PEC-walls.

a complete set of functions. In our case we assume PEC at the top and the bottom of the region, so the expansion in the y-direction can be carried out using Fourier series. The expansion in other directions may use a different series. For this paper we have chosen Legendre polynomials, but other choices are also possible. Also each field components can be treated separately.

To sum up, the functional expansion at each of the ports is derived for the local system of coordinates (x, y, z), shown in Figure 3, in the following form:

$$
\begin{aligned}
\vec{E}_t^{(k)}(x, y) &= \sum_{i=0}^{N_{Lx}^{(k)}} \sum_{j=0}^{N_{Tx}^{(k)}} \vec{i}_x a_{x,ij}^{(k)} e_{x,ij}(x, y) \\
&+ \sum_{i=0}^{N_{Ly}^{(k)}} \sum_{j=0}^{N_{Ty}^{(k)}} \vec{i}_y a_{y,ij}^{(k)} e_{y,ij}(x, y) \quad \text{for} \quad k = 1, 2 \\
\vec{E}_t^{(k)}(z, y) &= \sum_{i=0}^{N_{Lz}^{(k)}} \sum_{j=0}^{N_{Tz}^{(k)}} \vec{i}_z a_{z,ij}^{(k)} e_{z,ij}(z, y) \\
&+ \sum_{i=0}^{N_{Ly}^{(k)}} \sum_{j=0}^{N_{Ty}^{(k)}} \vec{i}_y a_{y,ij}^{(k)} e_{y,ij}(z, y) \quad \text{for} \quad k = 3, 4
\end{aligned}
\tag{22}
$$

where

$$
\begin{aligned}
e_{x,ij}(x, y) = L_i(x) \sin(j k_y y) \quad & e_{y,ij}(x, y) = L_i(x) \cos(j k_y y) \\
e_{z,ij}(z, y) = L_i(z) \sin(j k_y y) \quad & e_{y,ij}(z, y) = L_i(z) \cos(j k_y y)
\end{aligned}
\tag{23}
$$

The wave number for the trigonometric expansion along direction y is $k_y = \frac{\pi}{y_2 - y_1}$. The Legendre polynomials of i-th order $L_i(x)$, $L_i(z)$ can be calculated using the following expressions:

$$
L_i(x) = P_i\left(\frac{x - x_1}{x_2 - x_1}\right), \quad L_i(z) = P_i\left(\frac{z - z_1}{z_2 - z_1}\right)
$$

$$
P_i(t) = (-1)^i \sum_{k=0}^{i} \binom{i}{k} \binom{i+k}{k} (-t)^k
\tag{24}
$$

The overall number of expansion terms in the vectorial form (16) is:

$$
\begin{aligned}
N'_{Pk} &= \left(N_{Lx}^{(k)} + 1\right) N_{Tx}^{(k)} + \left(N_{Ly}^{(k)} + 1\right)\left(N_{Ty}^{(k)} + 1\right) \quad \text{for} \quad k = 1, 2 \\
N'_{Pk} &= \left(N_{Lz}^{(k)} + 1\right) N_{Tz}^{(k)} + \left(N_{Ly}^{(k)} + 1\right)\left(N_{Ty}^{(k)} + 1\right) \quad \text{for} \quad k = 3, 4
\end{aligned}
\tag{25}
$$

3. NUMERICAL RESULTS

In this section we shall illustrate the proposed reduction method through two numerical examples. All the computations were performed on a Intel i7 processor and 16-GB RAM employing curvilinear tetrahedral elements and the third order vector basis functions [16].

3.1. Example 1: Three-pole Combline Filter

The first case deals with a three-pole combline filter in the WR-90 waveguide, which has already been addressed in [18] using a hybrid Finite-Difference Mode-Matching method. It contains 8 axially symmetrical metallic posts of a radius 2 mm (all dimensions are provided in Figure 4(a)). The goal of the simulation was to compute the transmission and reflection coefficients over the range from 10 to 12 GHz assuming the TE_{10} mode excitation. The computational domain was discretized using 10193 curvilinear tetrahedral third order elements, which resulted in 177000 degrees of freedom and $1.35 \cdot 10^7$ nonzero elements in each of the FEM matrices. First, the filter was simulated by means of the standard FEM formulation without employing the reduction scheme in order to generate the reference results. The computation time for one frequency point is approximately 13 sec, which results in 661 sec (1309 sec) for the whole 51 (101) frequency point (fp) characteristic.
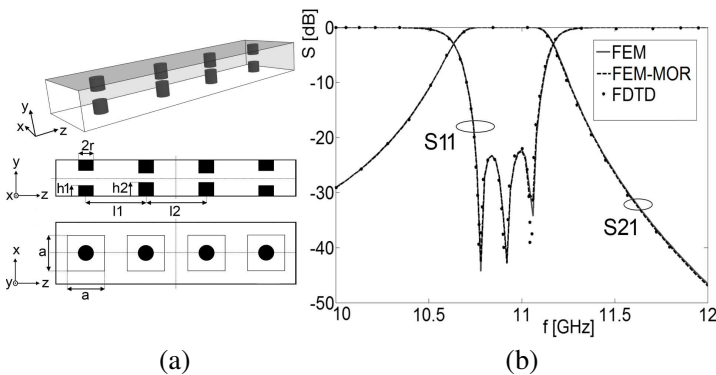

(a)   (b)

Figure 4. (a) The scheme of the WR-90 combline filter, $h_1 = 3.63$ mm, $h_2 = 4.53$ mm, $l_1 = 20.902$ mm, $l_2 = 19.802$ mm, $r = 2$ mm, $a = 14$ mm. (b) S-parameters of the filter computed using standard FDTD [18], FEM and FEM-MOR — the proposed MOR approach.

Then, the structure was analyzed by means of the proposed multilevel reduction scheme using the FEM mesh generated previously. Four cubicoid subregions were selected and separated from the rest of the computational domain using for each of them four fictitious walls of the dimension $14\,\text{mm} \times 10.16\,\text{mm}$, as shown in Figure 4(a). Each subregion contains two cylindrical posts. The tangential electric field on each of the walls was projected onto a subspace spanned by 10 orthogonal functions ($N'_{Pk} = 10$ for $k = 1 \ldots 4$). In effect, the number of variables at each of the subregion interfaces was reduced from approximately 1400 to 40. The tangential field on the input and output ports has been projected onto a subspace consisting only of the excitation mode — TE_{10}. Afterwards, the first level reduction was carried out in four subspaces using $q = 5$, which generated four macro-elements of the size 200×200. The interfaces for the second level reduction were selected so as to coincide with the input and output ports of the structure. As a result, the region which undergoes reduction at the second level consists of the four macro-elements created in the first reduction and the rest of the computational domain. We used the reduction order $q = 18$ and the number of variables at the external ports was $p = 2$, so the size of the resultant matrix after the second reduction was just 38. As the result of the proposed approach, the overall CPU time for 101 frequency points dropped from 1309 sec to 55 sec, which makes the present technique over 24 times faster than the original FEM (Table 1). Figure 4(b) depicts the S-parameters of the structure obtained by means of the proposed MOR approach compared with the standard FDTD [18] and FE methods. A very good agreement can be observed over the entire bandwidth.

Table 1. Comparison of the performance of the three-pole combline filter analysis for the standard FEM and the proposed algorithm a multilevel FEM-MOR.

	Standard FEM	FEM-MOR
Number of unknowns	177000	38
MOR time	-	55 sec
Simulation time for the whole characteristic at 51 (101) fp	661 (1309) sec	0.02 (0.04) sec
The speedup for 51 (101) fp	1	12 (24)

3.2. Example 2: Coupled-resonator Waveguide Filter

The next test involves computing the S-parameters of the TE_{10} mode excitation in a coupled-resonator waveguide filter (Figure 5(a)), whose

dimensions are provided in [19]. Instead of the metallic post in the center of the main cavity, we have used an incomplete-height bow-tie metallic post [20], which allows for tuning the filter.
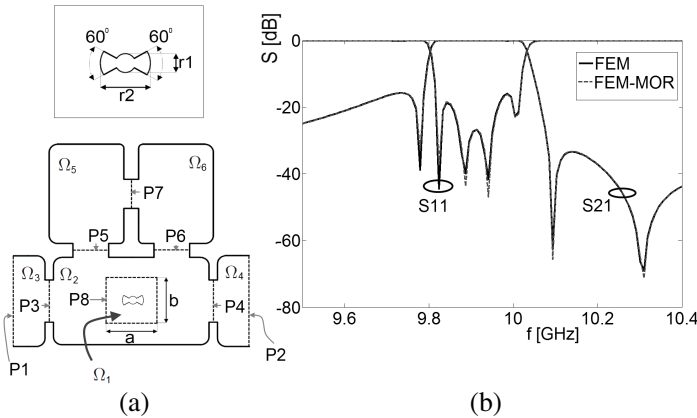

Figure 5. (a) The top view of the coupled-resonator waveguide filter, $r_1 = 1\,\text{mm}$, $r_2 = 2\,\text{mm}$, $a = 11.5\,\text{mm}$, $b = 10.5\,\text{mm}$. The height of the bow-tie post is $9\,\text{mm}$. (b) S-parameters of the filter computed using standard FEM and FEM-MOR.

We have analyzed the filter by means of the standard FEM, the two-level MOR (FEM-MOR2) and the three-level MOR (FEM-MOR3). As in the previous example, the results obtained by means of the standard FEM serve as a reference. In the FEM-MOR3 case the macro-element at the first, lowest level covered the $\underline{\Omega}_1$ subdomain in order to capture the behavior of the electric field in the vicinity of the bow-tie post. It is separated from the rest of the structure using four fictitious walls (P_8), on which the electric field is projected on the subspace spanned by 15 functions ($N'_{Pk} = 15$ for $k = 1 \ldots 4$). At the second level 5 subdomains are subject to the reduction: $\widetilde{\underline{\Omega}}_1 \cup \underline{\Omega}_2 \cup \underline{P}'_8$ and $\underline{\Omega}_3 \ldots \underline{\Omega}_6$. They were separated using internal ports placed in the middle of the irises ($\underline{P}'_3 \ldots \underline{P}'_7$). Each of them was projected onto a subspace spanned by 9 modes. At the third level the reduction covers the whole computational domain, this is to say, it includes: five macro-elements created at the second reduction level and the internal ports $\underline{P}_3 \ldots \underline{P}_7$. The interface for the macro-element created at the third reduction level is composed of the excitation ports P_1, P_2 on which the electric field is projected on the subspace spanned by 9 modes. In this case the proposed approach allowed us to achieve the

speedup by a factor of 27 † over the standard FEM (Table 2) and the S-parameters computed using both methods are almost indistinguishable (Figure 5(b)). In FEM-MOR2 the first reduction level is omitted, so this approach begins with creating 5 macro-elements: $\underline{\Omega}_1 \cup \underline{\Omega}_2 \cup \underline{P}'_8$ and $\underline{\Omega}_3 \ldots \underline{\Omega}_6$. The second reduction level is the same as the third level of the FEM-MOR3 case. Table 2 shows that FEM-MOR3 is more than 4 times faster than FEM-MOR2, which proves that in complex structures it is profitable to employ the functional expansion and the multilevel reduction.

Table 2. Comparison of the performance of the coupled-resonator waveguide filter analysis for the standard FEM and the proposed algorithm FEM-MOR2 and FEM-MOR3.

	Standard FEM	FEM-MOR2	FEM-MOR3
Number of unknowns	440000	234	234
MOR time(s)	-	1145	243
Simulation time for the whole characteristic at 51 (101) fp	3310 (6555) sec	0.24 (0.47) sec	0.24 (0.47) sec
The speedup for 51 (101) fp	1	3 (6)	13.6 (27)

4. CONCLUSION

In this paper a multilevel model order reduction method has been presented. The method involves creation of nested macro-elements and operates directly on the system of equations obtained using the standard FEM formulation. The efficiency of the reduction scheme is enhanced by means of the operation called the boundary compression, which is achieved via projection of the field onto a set of functions at the macro-element boundaries and gives the benefit of smaller macro-elements. Since the reduction and functional projection do not introduce any frequency-dependent terms into the system of equations, they are performed only once for the whole frequency sweep. The numerical tests prove that the proposed method results in significant reduction of the number of variables, the memory usage and the simulation time.

---

† The speedup value takes into account the time needed to create multilevel reduction.

ACKNOWLEDGMENT

REFERENCES

1. Dziekonski, A., A. Lamecki, and M. Mrozowski, "Tuning a hybrid GPU-CPU V-cycle multilevel preconditioner for solving large real and complex systems of FEM equations," *IEEE Antennas and Wireless Propagation Letters*, Vol. 10, 619–622, 2011.

2. Dziekonski, A., A. Lamecki, and M. Mrozowski, "A memory efficient and fast sparse matrix vector product on a GPU," *Progress In Electromagnetics Research*, Vol. 116, 49–63, 2011.

3. Fotyga, G., K. Nyka, and M. Mrozowski, "Efficient model order reduction for FEM analysis of waveguide structures and resonators," *Progress In Electromagnetics Research*, Vol. 127, 277–295, 2012.

4. Zhu, Y. and A. C. Cangellaris, "Macro-elements for efficient FEM simulation of small geometric features in waveguide components," *IEEE Trans. Microwave Theory Tech.*, Vol. 48, 2254–2260, Dec. 2000.

5. De la Rubia, V. and J. Zapata, "Microwave circuit design by means of direct decomposition in the finite-element method," *IEEE Trans. Microwave Theory Tech.*, Vol. 55, No. 7, 1520–1530, Jul. 2007.

6. Wu, H. and A. C. Cangellaris, "A finite-element domain-decomposition methodology for electromagnetic modeling of multilayer high-speed interconnects," *IEEE Transactions on Advanced Packaging*, Vol. 31, No. 2, 339–350, May 2010.

7. Lee, S.-H. and J.-M. Jin, "Adaptive solution space projection for fast and robust wideband finite-element simulation of microwave components," *IEEE Microwave and Wireless Components Letters*, Vol. 17, No. 7, 474–476, Jul. 2007.

8. Fotyga, G., K. Nyka, and L. Kulas, "A new type of macro-elements for efficient two-dimensional FEM analysis," *IEEE Antennas and Wireless Propagation Letters*, Vol. 10, 270–273, Apr. 2011.

9. Podwalski, J., P. Kowalczyk, and M. Mrozowski, "Efficient multiscale finite difference frequency domain analysis using

multiple macromodels with compressed boundaries," *Progress In Electromagnetics Research*, Vol. 126, 463–479, Apr. 2012.

10. Kulas, L., P. Kowalczyk, and M. Mrozowski, "A novel modal technique for time and frequency domain analysis of waveguide components," *IEEE Microwave and Wireless Components Letters*, Vol. 21, No. 1, 7–9, Jan. 2011.

11. Kulas, L. and M. Mrozowski, "A fast high-resolution 3-D finite-difference time-domain scheme with macromodels," *IEEE Trans. Microwave Theory Tech.*, Vol. 52, No. 9, 2330–2335, Sep. 2004.

12. Kulas, L. and M. Mrozowski, "Multilevel model order reduction," *IEEE Microwave and Wireless Components Letters*, Vol. 14, No. 4, 165–167, Apr. 2004.

13. Fotyga, G., P. Kowalczyk, L. Kulas, K. Nyka, J. Podwalski, and M. Mrozowski, "Reduced order models in computational electromagnetics (in memory of Ruediger Vahldieck)," *2012 Asia-Pacific Symposium on Electromagnetic Compatibility (APEMC)*, 705–708, May 2012.

14. Sheehan, B. N., "ENOR: Model order reduction of RLC circuits using nodal equations for efficient factorization," *Proc. IEEE 36th Design Autom. Conf.*, 17–21, Jun. 1999.

15. Pelosi, G., R. Coccioli, and S. Selleri, *Quick Finite Elements for Electromagnetic Waves*, 2nd Edition, Artech House Antenna Library, 2009.

16. Ingelstrom, P., "A new set of H(curl)-conforming hierarchical basis functions for tetrahedral meshes," *IEEE Trans. Microwave Theory Tech.*, Vol. 54, No. 1, 106–114, Jan. 2006.

17. Dziekonski, A., P. Sypek, A. Lamecki, and M. Mrozowski, "Finite element matrix generation on a GPU," *Progress In Electromagnetics Research*, Vol. 128, 249–265, 2012.

18. Kusiek, A. and J. Mazur, "Application of hybrid finite-difference mode-matching method to analysis of structures loaded with axially symmetrical posts," *Microwave and Optical Technology Letters*, Vol. 53, No. 1, 189–194, Jan. 2011.

19. Szydlowski, L., A. Lamecki, and M. Mrozowski, "Coupled-resonator waveguide filter in quadruplet topology with frequency-dependent coupling a design based on coupling matrix," *IEEE Microwave and Wireless Components Letters*, Vol. 22, No. 11, 553–555, Nov. 2012.

20. Lech, R. and J. Mazur, "Tunable waveguide filter with bow-tie metallic posts," *IEE Proceedings Microwaves, Antennas and Propagation*, Vol. 151, No. 2, 156–160, Apr. 2004.